A99-31490

AIAA 99–2816

Large-Eddy Simulation of Turbulent Premixed Flames in the Thin Reaction Zone Regime

Won-Wook Kim and Suresh Menon
School of Aerospace Engineering
Georgia Institute of Technology
Atlanta, Georgia 30332-0150

35th AIAA/ASME/SAE/ASEE Joint Propulsion Conference and Exhibit
June 20-23, 1999 / Los Angeles, California

Large-Eddy Simulation of Turbulent Premixed Flames in the Thin Reaction Zone Regime

Won-Wook Kim* and Suresh Menon†
School of Aerospace Engineering
Georgia Institute of Technology
Atlanta, Georgia 30332-0150

A broadened-flame model has been developed for large-eddy simulation (LES) of premixed turbulent flows in the thin reaction zone regime. To validate the model, *a posteriori* tests in a gas turbine combustor (General Electric's lean premixed dry low NOx LM6000) has been carried out. A flamelet model for the premixed flame is combined with a dynamic model for the subgrid kinetics energy and two different turbulent flame speed models to simulate the propagation of the turbulent flame in this high swirl and high Reynolds number flow field. The conventional thin flame approach and the new broadened-flame approach are compared. Comparison of the computed results with experimental data shows that the broadened-flame model can significantly improve the results.

1 Introduction

The flamelet assumption describes a regime in premixed combustion that is often encountered in practical combustion devices. Within the flamelet assumption, the flame thickness δ is small (i.e., thin flame) compared to the smallest dynamic scale (i.e., the Kolmogorov scale η) of turbulence and the characteristic burning time τ_c is small compared to the characteristic flow time τ_t. As a result, the flame structure remains laminar and propagates as a thin front at a speed dictated by the mixture properties. In this regime, the turbulence only wrinkles and convects the flame without affecting its structure.

A model equation that describes the propagation of thin flames by convective transport and normal burning (self propagation by Huygens' principle) is the G-equation.[1,2] As discussed by Peters,[3] other flamelet models for the flame surface density can be constructed starting from the G-equation. Here, we consider a conservative form of G-equation which can be written as:

$$\frac{\partial \rho G}{\partial t} + \frac{\partial \rho u_i G}{\partial x_i} = -\rho S_L |\nabla G| \qquad (1)$$

where $G(x_i, t)$ is the progress variable, u_i $(i = 1, 2, 3)$ is the velocity, S_L is the local unstretched laminar flame speed, ρ is the mass density, t is the time, and x_i is the coordinate. In the flow field, the value of G is prescribed in the range [0,1]. Here, G is assigned the value of unity in the unburned region and zero in the burnt region with the thin flame identified by a fixed value of $0 \leq G_0 \leq 1$. Therefore, Eq. (1) describes the kinematic balance between convection of a level surface (defined as $G = G_0$) by the fluid velocity and the normal propagation at a speed S_L. In this flamelet model, the flame structure is effectively ignored since only the propagating surface is modeled. As a result, the details on reaction rates and species diffusion are not needed, which reduces the required computational effort considerably.

The burning speed appearing in Eq. (1) is defined with respect to the unburned mixture. Using mass conservation through the flame,[1] the term in Eq. (1) can be rewritten by replacing ρS_L with $\rho_o S_L^o$. Here, ρ_o is the reference reactant density and S_L^o is the undisturbed laminar flame speed. Note that S_L^o is constant while S_L increases through the flame.

When a constant laminar flame speed S_L^o is employed, the effects of flame stretch (which include contributions from tangential strain rate in the plane of the flame and flame curvature) are excluded. In the past, many attempts were made to include the effects of flame stretch induced by the mean flow[4] and curvature effects.[5] However, in the present formulation, flame stretch is implicitly modeled when the turbulent flame speed is determined. This approach can be justified since the major effect of flame stretch is to modify the local burning rate through changes in the diffusive processes.

The present study is focussed on developing models for large-eddy simulations (LES). In LES, fluid motion larger than the grid are resolved by solving the spatially filtered governing equations. Upon filtering (using the spatial filter as defined in Appendix A) Eq. (1), the following G-equation for LES is obtained:

$$\frac{\partial \overline{\rho}\widetilde{G}}{\partial t} + \frac{\partial \overline{\rho}\widetilde{u}_i\widetilde{G}}{\partial x_i} = -S^{sgs} - \frac{\partial}{\partial x_i}(G_i^{sgs}). \qquad (2)$$

The subgrid terms representing, respectively, the filtered source term and the unresolved transport term

*Post-Doctoral Fellow, AIAA Member
†Professor, AIAA Senior Member

are

$$\begin{cases} S^{sgs} = \overline{\rho_o S_L^o |\nabla G|} \\ G_i^{sgs} = \overline{\rho}[\widetilde{u_i G} - \widetilde{u}_i \widetilde{G}]. \end{cases} \quad (3)$$

The unresolved transport term is usually modeled using a gradient-diffusion assumption,[6]

$$G_i^{sgs} = \overline{\rho}[\widetilde{u_i G} - \widetilde{u}_i \widetilde{G}] \approx -\frac{\overline{\rho}\nu_t}{Sc^G} \nabla \widetilde{G} \quad (4)$$

where Sc^G is a turbulent Schmidt number (it is usually prescribed close to unity but can be calculated as a part of the solutions using the dynamic procedure as described in Appendix B). The source term for the filtered G-equation is approximated as,

$$S^{sgs} = \overline{\rho_o S_L^o |\nabla G|} \approx \rho_o S_T |\nabla \widetilde{G}| \quad (5)$$

where S_T is the turbulent flame speed averaged over a characteristic LES cell volume. This speed is not known explicitly and, therefore, must be modeled.

Although many models for S_T have been proposed in the past, here we consider two typical flame speed models. The first model is the Renormalization Group (RNG) model proposed by Yakhot:[7]

$$U_T = \exp\left[\frac{U_p^2}{U_T^2}\right] \quad (6)$$

where $U_T = S_T/S_L$, $U_p = u'/S_L$ and u' is the turbulence intensity. This model estimates the increased flame speed due to flame wrinkling and provides an elegant closure for the LES equation provided u' can be determined (which is possible using the subgrid kinetic energy model described in Appendix A). This model also compares well with experimental data in the low to moderately high u'/S_L range.[8] Two unique features make this model particularly attractive from LES standpoint. First, this model predicts the rapid increase in S_T/S_L at low u'/S_L and then a gradual *bending* at higher u'/S_L consistent with data. Second, Eq. (6) includes no adjustable parameters to fine-tune. This feature may also be a disadvantage when the model does not properly fit experimental data. For example, some discrepancy between the model prediction and data was noted by Ronney and Yakhot[9] even at low U_p.

The second model considered here is a model proposed by Pocheau[10] who argued that Yakhot's model is an approximate solution obtained by a renormalization procedure applied to the Clavin-Williams relation:[11]

$$\frac{S_T}{S_L} = 1 + \frac{u'^2}{S_L^2} \quad (7)$$

which is valid only at low turbulence intensity level. Pocheau[10] derived an exact solution from a renormalization procedure of the Clavin-Williams relation which is scale invariant in the following form:

$$U_T = \left(1 + \beta U_p^\gamma\right)^{1/\gamma} \quad (8)$$

where $\gamma = 2$ is chosen to conserve energy and β is an adjustable parameter. Both these flame models have been successfully used for various turbulent premixed problems[6,12,13] primarily for thin flames in low-to-moderate u'/S_L regimes.

However, for high u'/S_L when some turbulent scales are smaller than the flame thickness, these models are not directly applicable. The present study describes a new model that is valid over a wide range of u'/S_L values and is particularly suited for LES. Application of this model in LES of high Reynolds number flow is also described in this paper.

2 Rationale for Broadened-Flame Models

The propagation of premixed flames in turbulent flows in the thin flame limit can be modeled using a laminar flame model such as the G-equation model (1) (with the laminar flame speed S_L) if all the turbulent scales down to the Kolmogorov scale are resolved and this Kolmogorov scale is considerably larger than the flame thickness (i.e., $\eta > \delta$). When all the turbulent scales are not resolved (as in a LES) but $\eta > \delta$ then the filtered equation (2) can be used to simulate the turbulent flame by employing closure models such as the ones shown in (4) and (5).

However, if turbulent scales smaller than δ exist in the flow then these scales will disturb the flame structure thereby invalidating the thin-flame assumption used in the above noted models. A major effect of turbulent scales smaller than δ is a broadened flame[9] with a characteristic thickness larger than δ (denoted here as δ^*). As a result of the increased transport by turbulence within the broadened flame, the laminar flame speed of the broadened flame (denoted here as S_L^*) will also increase from its undisturbed laminar value of S_L. Analogous to the thin flames, the broadened flame will be wrinkled by turbulent fluctuations (denoted here as u'^*) corresponding to scales larger than δ^*. The characteristic broadened-flame properties such as δ^*, S_L^*, and u'^* need to be determined in order to incorporate this effect into LES models.

The broadened flame belongs to the distributed reaction zone regime according to the classical classification. In this regime, the turbulent scales are smaller than the flame thickness and begin to penetrate into the flame structure and, therefore, strong flame-turbulence interactions exist. Peters[5] recently argued that the small scales penetrate and broaden mostly the chemically inert preheat zone which extends into the unburned mixture but do not reach and modify the reaction zone before dissipating. Based on this argument, he called this regime the thin reaction zone regime. The existence of the thin reaction zone regime has also been observed in experiments.[14–16] This regime was also called an extended flamelet regime[17] based on DNS results.

Regardless of its designation and although this regime is a flamlet-type regime, conventional flamelet models cannot be directly used. The new model discussed here to account for flame broadening attempts to deal with both the flamelet and the thin-reaction zone regimes under one unifying formulation.

Inclusion of the flame broadening is even more important for practical applications since it can predict the leveling of the constant Reynolds number curves at high u'/S_L in the plot of S_T/S_L versus u'/S_L. This behavior has been observed in many situations. Although the dominating influences are not precisely known, Ronney[18] suggested four possible reasons. The first is a possible subtle change in the exponent in Eq. (6) obtained kinematic arguments. The second may be due to gas expansion and flame instability, which has been shown to be important at low u'/S_L but may play a diminishing role at higher u'/S_L. The third reason may be due to high flame stretch which, in general, reduces the local burning rate. And finally, the fourth reason may be due to a transition from flamelet to distributed combustion where $S_T \sim \sqrt{u'}$. Proper accounting for this experimentally observed behavior is critical since otherwise S_T/S_L will be significantly overestimated for high u'/S_L.

If flame broadening effect is included correctly then the turbulent flame speed will increase due to fluctuations at scales smaller than the integral length but larger than the broadened-flame thickness δ^*. When δ^* increases for a fixed integral length scale, the range of scales that contribute to increasing the flame speed decreases. When δ^* becomes larger than the integral length, the effective turbulent flame speed becomes equal to the S_L^* and $S_T/S_L^* = 1$ (but note that $S_T/S_L \neq 1$). S_L^* will also increase with increasing u' since more turbulent scales are involved in increasing the transport rates within the broadened flame. The inclusion of these features within a model is investigated in the next two sections.

3 A Broadened-Flame Model

Ronney and Yakhot[9] have obtained a relation between S_L^* and S_L by assuming Kolmogorov turbulence:

$$\frac{S_L}{S_L^*} = \left(X^2 - 2X + 2\right)^{1/2} \tag{9}$$

where $X = (\delta^*/\eta)^{2/3} = 0.205 Re_2^{1/2} (\delta^*/\ell)^{2/3}$ and it can be obtained by solving

$$\left[\frac{28.1}{A^2}\left(1 - \frac{n^{2/3}}{Re_2^{1/2}}\right)\frac{Re_2^{1/2}}{U_p^2}\right] X^3 - X^2 + 2X - 2 = 0. \tag{10}$$

In the above relations, $Re_2 = \varepsilon^{1/3}\ell^{4/3}/\nu$ and $n \approx 10.76$ is a constant which appears in $\eta/\ell = nRe_2^{-3/4}$. They also derived a relation between u'^* and S_L:

$$\left[\frac{u'^*}{S_L}\right]^2 = \frac{1 - n^{2/3}Re_2^{-1/2}X}{1 - n^{2/3}Re_2^{-1/2}} U_p^2 \tag{11}$$

and between δ^* and S_L^*:

$$\delta^* = A\alpha^*/S_L^*. \tag{12}$$

Here, A is a constant to be determined and α^* is the turbulent thermal diffusivity.

Typically, thin flame models provide a relationship between S_T/S_L and u'/S_L. Thus, assuming that the same functional relationship holds in the thin reaction zone regime and substituting these variables with S_T/S_L^* and u'^*/S_L^*, one can obtain the flame speed model which includes the flame broadening effects due to high U_p. Any thin flame speed model can be employed for this purpose. For example, Ronney and Yakhot[9] combined Yakhot's model with (9) and (11) to obtain

$$U_T = \left(X^2 - 2X + 2\right)^{1/2} \exp\left[\frac{1 - n^{2/3}Re_2^{-1/2}X}{1 - n^{2/3}Re_2^{-1/2}}\left(\frac{U_p^2}{U_T^2}\right)\right]. \tag{13}$$

This model is applicable only for $X \leq n^{-2/3}Re_2^{1/2}$. When $X = n^{-2/3}Re_2^{1/2}$ (i.e., $\ell = \delta^*$), the exponent in Eq. (13) becomes zero and, therefore, this model cannot be used for $X > n^{-2/3}Re_2^{1/2}$. This limit of applicability is physically justified since for $X > n^{-2/3}Re_2^{1/2}$ all turbulent scales lie inside the broadened flame and no turbulent energy can exist in scales larger than ℓ (note that ℓ is usually determined by the largest turbulent scale of the problem). Thus, the turbulent flame speed cannot further increase in this regime.

However, the above explanation is no longer valid when LES is considered. In LES, the characteristic length scale for subgrid turbulence is the largest unresolved scale by the grid size instead of the integral length scale which is determined by physical arguments or geometry of problems. Therefore, a broadened-flame model for LES needs to be defined in terms of the the grid resolution. In this subgrid approach, the broadened-flame thickness can be larger than the grid resolution and the turbulent scales larger than the grid resolution can further increase the broadened-flame speed. To take this feature into account within the framework of LES, a modification to the above model is needed.

4 A Broadened-Flame Model for LES

A broadened-flame model consistent with LES concepts implies that only information available from the subgrid turbulence model should be used. To date, most subgrid models use the eddy-viscosity assumption and are based either on the algebraic model by

Smagorinsky[19] or the one-equation model for the subgrid kinetic energy by Schumann.[20] For LES of non-reacting flows using reasonable grid resolutions, the effects of either subgrid model on the statistical quantities are usually marginal. However, for LES of reacting flows, as discussed by Fureby[21] in his recent review paper, the one-equation model and its derivatives (i.e., dynamic versions) appear to be superior when compared to the dynamic algebraic model.[22] In addition, the subgrid kinetic energy naturally provides an estimate for the subgrid turbulence intensity (which is unavailable when using the algebraic model). For these reasons, the present formulation is based on the one-equation model. This model is briefly discussed in Appendix A.

In the following, we extend the earlier approach discussed in the previous section and obtain relations between δ^*, S_L^*, and u'^* for LES applications In the one-equation model, the subgrid eddy viscosity is obtained by

$$\nu_t = C_\nu (k^{sgs})^{1/2} \overline{\Delta} \tag{14}$$

where $k^{sgs} = \frac{1}{2}[\widetilde{u_k^2} - \widetilde{u}_k^2]$ is the subgrid kinetic energy and $\overline{\Delta}$ is the grid width which represents the characteristic length scale for the subgrid quantities. The subgrid turbulence intensity is related to k^{sgs}: $u' = \sqrt{2k^{sgs}/3}$ and the subgrid dissipation term in the kinetic energy model is:

$$\varepsilon^{sgs} = C_\varepsilon \frac{(k^{sgs})^{3/2}}{\overline{\Delta}}. \tag{15}$$

By combining (14) and (15) we obtain:

$$\frac{\nu_{total}}{\nu} = \frac{\nu_t + \nu}{\nu} = \frac{C_\nu}{C_\varepsilon^{1/3}} Re_2 + 1 \tag{16}$$

where Re_2 is redefined similarly but using the subgrid quantities: $Re_2 = (\varepsilon^{sgs})^{1/3}\overline{\Delta}^{4/3}/\nu = 1.5^{1/2} C_\varepsilon^{1/3} u' \overline{\Delta}/\nu$. For arbitrary scale δ^* and corresponding ν^*, Eq. (16) can be rewritten as

$$\frac{\nu^*}{\nu} = \frac{C_\nu}{C_\varepsilon^{1/3}} Re_2 \left(\frac{\delta^*}{\overline{\Delta}}\right)^{4/3} + 1. \tag{17}$$

If it is assumed that flame broadening is resulted primarily due to increased rates of heat and mass transport with no change in characteristic chemical reaction times (this assumption is valid as long as the thin reaction zone of the premixed flame remains free of turbulent disturbances), then this leads to Damköhler's hypothesis:[23]

$$\frac{S_L^*}{S_L} = \left(\frac{\alpha^*}{\alpha_L}\right)^{1/2} \tag{18}$$

where α^* is the turbulent thermal diffusivity based on scales smaller that δ^* and α_L is the molecular thermal diffusivity. Using the following identity

$$\frac{\alpha^*}{\alpha_L} = \frac{\nu^*}{\nu} \frac{\mathrm{Pr}_L}{\mathrm{Pr}^*} \tag{19}$$

Eqs. (18) and (19) can be combined assuming $\mathrm{Pr}_L / \mathrm{Pr}^*$=1 (here, Pr is the Prandtl number) to obtain a relation between ν^* and S_L^*:

$$\frac{S_L^*}{S_L} = \left(\frac{\nu^*}{\nu}\right)^{1/2}. \tag{20}$$

Finally, Eq. (17) can be rewritten in terms of S_L^*/S_L using (20) resulting in a relation between δ^* and S_L^*:

$$\left(\frac{S_L^*}{S_L}\right)^2 = C_1 Re_2 \left(\frac{\delta^*}{\overline{\Delta}}\right)^{4/3} + 1 \tag{21}$$

where $C_1 = C_\nu / C_\varepsilon^{1/3}$.

The turbulent scales smaller than δ^* contribute to increase the laminar flame speed to S_L^* and to broaden the flame. On the other hand, the turbulent scales larger than δ^* can wrinkle the broaden flame inside the each LES cell and, therefore, will further increase the burning speed to S_T. When $\delta^* \geq \overline{\Delta}$, all the turbulence inside the LES cell will contribute only to broaden the flame and, hence, the the burning speed at that location will be S_L^*.

To close the problem, another relation between δ^* and S_L^* is required. By analogy with laminar flames, the natural choice is the relation shown in (12). This relation can be rewritten in the form

$$\frac{S_L^*}{S_L} = \frac{1}{C_2} \frac{\delta^*}{\overline{\Delta}} \tag{22}$$

where $C_2 = AU_p/(PrRe_1) = A\nu/(\mathrm{Pr}\,\overline{\Delta} S_L)$ and $Re_1 = u'\overline{\Delta}/\nu = Re_2/(1.5^{1/2} C_\varepsilon^{1/3})$. Combining (21) and (22) results in the following algebraic equation for S_L^*/S_L

$$\left(\frac{S_L^*}{S_L}\right)^2 = C_3 \left(\frac{S_L^*}{S_L}\right)^{4/3} + 1 \tag{23}$$

where $C_3 = C_1 C_2^{4/3} Re_2$. This algebraic equation can be easily solved for known Re_2 (i.e., u') resulting in the following solution:

$$\frac{S_L^*}{S_L} = \frac{1}{27}\left(9C_4 + \frac{C_3^2}{C_4} + 3C_3\right)^{3/2} \tag{24}$$

where $C_4 = \left[\frac{1}{2} + \frac{1}{27}C_3^3 + \frac{1}{18}\left(81 + 12C_3^3\right)^{1/2}\right]^{1/3}$

It remains only to determine u'^*, the turbulence intensity based only on scales between $\overline{\Delta}$ and δ^*. This is accomplished by subtracting (15) from itself with $\overline{\Delta}$ replaced by δ^*:

$$\frac{u'^*}{S_L} = \frac{u'}{S_L}\left[1 - \left(C_2 \frac{S_L^*}{S_L}\right)^{2/3}\right]^{1/2} \tag{25}$$

where $C_2 S_L^*/S_L = \delta^*/\overline{\Delta}$ and, therefore, $u'^*/S_L \geq 0$ (since $u'^* = 0$ if $\delta^* \geq \overline{\Delta}$).

This broadened-flame model can be applied to any turbulent flame speed model. A turbulent broadened-flame speed model is obtained by substituting (24) and (25) into the broadened-flame version of Yakhot's model:

$$\left(\frac{S_T}{S_L}\right) = \left(\frac{S_L^*}{S_L}\right) \exp\left[\left(\frac{u'^*}{S_L}\right)^2 / \left(\frac{S_T}{S_L}\right)^2\right] \tag{26}$$

or into the Pocheau's model:

$$\left(\frac{S_T}{S_L}\right)^\gamma = \left(\frac{S_L^*}{S_L}\right)^\gamma + \beta\left(\frac{u'^*}{S_L}\right)^\gamma. \tag{27}$$

In (27), the first term (R_1) on the right hand side represents the increase in the burning speed due to the flame broadening and the second term (R_2) represents the contribution by the turbulence whose scale is larger than the broadened flame thickness. It is important to note that in the limit of $u' \to 0$, both u'^*/u' and S_L^*/S_L become unity and, therefore, the original thin flame models are recovered.

Several parameters such as Pr, C_ν, C_ε, β, γ and A appear in the above formulations. The Prandtl number is a property of the flow and is usually, $Pr = 0.72$. Also, C_ν and C_ε are model coefficients in Eqs. (14) and (15). These parameters can be determined theoretically using the RNG method. For example, Yakhot and Orszag[24] calculated $C_\nu \approx 0.05$ and $C_\varepsilon \approx 1.68$ from the RNG theory. A dynamic approach to compute these coefficients locally in time and space is also available.[13,25,26] The parameter β can be obtained by fitting experimental data on turbulent flame speed. β can be determined by a dynamic procedure as well. This procedure is discussed in Appendix B. For Pocheau's model, $\gamma = 2$ based on energy conservation and the parameter A which appears in the relation between δ^* and S_L^* (12) has been estimated by Ronney and Yakhot[9] to be ≈ 6 based on comparison with the joint-pdf computations of Pope and Anand.[27] This value is employed here without any further fine-tuning.

The present model can be applied in the entire regime where the flamelet assumption including the extended version (i.e., the thin reaction zone regime) holds. Within this regime, regardless of the grid resolution, the broadened-flame thickness δ^* can be of any size and can be even larger than the grid resolution. In that case, the subgrid-scale turbulence contributes only to flame broadening and the flame speed is determined by the first term R_1 on the right hand side of (27) while the second term R_2 becomes zero. However, at very high turbulence intensities (i.e., when turbulence starts to penetrate the thin reaction zone), flame stretch and local quenching often leads to global extinction.[28] Flamelet models cannot be used beyond this limit even if flame broadening effects are included. Therefore, a domain of applicability for the flame broadening model needs to identified as described in the next section.

5 Applicable Regime for Broadened-Flame Models

By rearranging (23), one can obtain the following relation between u'/S_L and $\delta^*/\overline{\Delta}$:

$$\frac{u'}{S_L} = \frac{PrRe_1}{A} \frac{\frac{\delta^*}{\overline{\Delta}}}{\left[C_5 Re_1 \left(\frac{\delta^*}{\overline{\Delta}}\right)^{4/3} + 1\right]^{1/2}} \tag{28}$$

where $C_5 = 1.5^{1/2} C_\varepsilon^{1/3} C_1$. Using simple turbulence theory[29]

$$\frac{\overline{\Delta}}{\eta} = nRe_1^{3/4} \tag{29}$$

Eq. (28) can be rewritten using Kolmogorov length scale η instead of $\overline{\Delta}$:

$$\frac{u'}{S_L} = \frac{PrRe_1^{1/4}}{nA} \frac{\frac{\delta^*}{\eta}}{\left[\frac{C_5}{n^{4/3}} \left(\frac{\delta^*}{\eta}\right)^{4/3} + 1\right]^{1/2}} \tag{30}$$

where n is a constant which can be estimated based on the RNG theory: $n = 0.123$. Once δ^*/η is given for a known Reynolds number, the corresponding u'/S_L also can be found.

To determine the regime of applicability, the structure of the flame needs to be considered. The flame is believed to be composed of three subregimes. The first subregime is a chemically inert preheat zone which is followed in sequence by a thin inner layer[30] and a post-flame oxidation layer. All reaction processes occur inside the thin inner layer and thickness of this subregime is believed to be an order of magnitude smaller than the flame thickness. Peters[5] estimated this thickness using the two-dimensional numerical simulation data[17] of laminar premixed flame interacting with a vortex pair. In this simulation, the flame fronts were shown to be resistant to flame stretch for Karlovitz numbers of 180 for the case without heat loss. This value corresponds to a reaction zone thickness of 0.07 times smaller than the flame thickness.

If the Kolmogorov scale is smaller than the thickness of this inner layer, the flame breaks up and the flamelet assumption (even in extended sense) is no longer valid. Therefore, by substituting $\eta = 0.07\delta^*$ into (30), one can estimate the turbulent fluctuation limit for the flamelet model (note that this estimation is not dependent on the turbulent flame speed model employed) as follows,

$$\frac{u'}{S_L} = 2.33 Re_1^{1/4}. \tag{31}$$

This flame assumption limit agrees well with the quenching limit by Abdel-Gayed and Bradley[31,32] obtained from studies of quenching in fan-stirred explosion vessels. They observed that for $Re_1 > 300$,

partial quenching occurs when $u'/S_L = 2Re_1^{1/4}$ and total flame quenching when $u'/S_L = 3Re_1^{1/4}$.

Quenching is not solely dependent on flame stretch due to turbulent eddies or mean strain. Other physical processes such as thermal processes also affect flame quenching. However, for high intensity of turbulence, the flame stretch due to turbulent eddies probably does play a major role in flame quenching. Figure 1(a) shows the comparison between the flamelet limit predicted by the present model and the quenching limit observed in experiments.[33] Clearly the present model gives an excellent estimate of the quenching limit. This curve also identifies the upper limit of applicability of the present broadened-flame model.

Figure 1(b) and (c) show the turbulent flame speed (S_T/S_L) plots as predicted by the broadened-flame model (27) in terms of turbulence intensity u'/S_L for various Re_1. Fig. 1(b) shows plots for Re_1 in the range from 1 to 50 and Fig. 1(c) shows the flame speed variation for Re_1 up to 10,000. Each curve is plotted in the range of turbulence intensity where the flamelet assumption is valid as determined by (31). For $Re_1 = 1$, the turbulent flame speed is solely determined by the broadened laminar flame speed (R_1) in the entire range of u'/S_L. For higher Re_1, the increased flame speed due to the unresolved subgrid-scale turbulence (R_2) is added to this broadened laminar flame speed and the final turbulent flame speed is determined based on these two contributions. The R_2 contribution (which appears as a hump at lower intensity) is estimated using Pocheau's model with $\beta = 20$ and $\gamma = 2$. These parameters are obtained by matching the model with the experimental data on methane(CH_4)/air and ethylene(C_2H_4)/air flames.[34] These experiments were arbitrary chosen and different sets of experimental data will result in different optimal values for the parameters. Therefore, the parameters need to be calibrated for case by case which is not elegant from computational standpoint. As an alternate to this approach, a dynamic calibration of the parameters (as a part of the simulation) is suggested and briefly described in Appendix B.

The sharp discontinuity in each curve for Re_1 up to 200 indicates where $\delta^* = \overline{\Delta}$. For higher turbulence intensity above this discontinuity, the flame speed is again solely determined by the broadened-flame speed (R_1). For the range where the turbulent flame speed is solely determined by R_1, a higher flame speed is observed for lower Re_1 at the same u'/S_L. This is reasonable since lower Re_1 with the same u'/S_L implies that smaller grid width is involved. Therefore, if compared on the same grid, lower Re_1 case belongs to higher turbulence intensity location (i.e., broader flame region where the burning speed is faster). For Re_1 higher than 500, the range where the turbulent flame speed is solely determined by R_1 disappears.

6 Results and Discussion

The results of the current LES are discussed in this section. Nine different test models are studied as summarized in Table I. The first letter in the name of test models (for example, "P" in the test model PBD20) indicates which turbulent flame speed model is employed ("Y" for Yakhot's model and "P" for Pocheau's model). The second letter indicates either the broadened-flame model ("B") or the conventional thin flame model ("T"). In the broadened-flame model, the applicability limit was applied, as discussed in the previous section. In the conventional thin flame model, a maximum value of u'/S_L is prescribed to prevent overestimation of turbulent flame speed at high u'/S_L. Above this maximum u'/S_L, turbulent flame speed is assumed to be constant. Following earlier studies,[6,13] the maximum u'/S_L is set to be 20 for Yakhot's model and 16.6 for Pocheau's model. The third letter indicates if the dynamic model (to determine the turbulent Schmidt number Sc^G as described in Appendix B) is employed. If the dynamic model is used, the letter will be "D". Otherwise, it will be "C" which stands for constant turbulent Schmidt number. The number in the last place indicates the value of the adjustable parameter β in Pocheau's model and, therefore, only appears in cases based on Pocheau's model. Various values of β (i.e., 2, 10, 20, and 30) were tested. These values were chosen based on our earlier study[13] where β was calibrated using the experiment[34] of stabilized turbulent premixed flames by a weak swirl or by a stagnation plate. It was observed that $\beta = 20$ case compares well with the experiment. Table I also shows time period where time average has been taken. The time period is summarized in terms of flow-through times (T_{flow}) based on the mean centerline axial velocity at the inlet. The implication of this flow-through time is discussed later.

The computational domain is the combustor downstream of the dual annular counter-rotating swirler premixer. This configuration is a part of General Electric Aircraft Engine (GEAE) company's lean premixed dry low NOx emissions LM6000 gas turbine combustor.[35] Only reacting LES was conducted and the results are compared with the experimental data provided by GEAE. (Nonreacting LES implemented in a similar combustor can be found elsewhere.[13]) A schematic of the LM6000 gas turbine combustor is shown in Figure 2. (Note that scale of the combustor is slightly different from the combustor we studied earlier.[13]) A highly swirling jet (the maximum value of tangential velocity component is slightly greater than the peak value of axial velocity component) is injected from a circular inlet under high pressure (P_f=6.18x10^5 N/m^2, i.e., $P_f \approx 6$ atmospheres) and temperature (T_f=644 K) conditions. The combustor comprises of a rectangular box with two blocks located at top and bottom surfaces from which cool-

ing air is blown downstream. The Reynolds number based on the inlet mean streamwise velocity and the inlet jet diameter D_0, is 350,000. The premixed fuel-air mixture has a prespecified laminar flame speed of 0.28 m/sec (corresponding to a lean methane-air mixture). Estimated flame temperature is around T_p=1807 K (based on gaseous emissions). The swirl number $S = \int_0^R \rho u w r^2 dr / R \int_0^R \rho u^2 r dr$ is about 0.56. The radial number $R = \int_0^R \rho u v r dr / \int_0^R \rho u^2 r dr$ which represents the effect of inlet radial velocity is 0.012.

The Reynolds number is high enough that fully developed turbulence can be assumed. Observations suggest that the ratio u'/S_L can be locally as large as 100's in this combustor. Using nondimensional parameters to characterize flame-turbulence interactions, several regimes of interest can be identified.[3] Typically, Re, Da, and Ka are used for this purpose. Here, $Re = u'\ell/\nu$ (where ℓ is the integral length scale, approximated here by the inlet jet diameter D_0), $Da = \tau_t/\tau_c$ is the Damköhler number (which is defined as a ratio of a characteristic flow time τ_t to a characteristic chemical reaction time τ_c), and $Ka = (\delta_L/S_L A)\, dA/dt$ (where $(1/A)\, dA/dt$ is the incremental change in flame surface area due to flame stretch) is the turbulent Karlovitz number which is defined to provide a measure of flame stretch. In the present case, $Re = 110,000$, $Da = 8$, and $Ka = 42$. According to Peters[5] the present problem belongs to the thin reaction zone regime. This problem, therefore, is a good test case to validate the broadened-flame model.

Earlier, we studied a similar combustor under almost identical flow conditions[13,36] using a conventional thin flame model based on G-equation. This approach was justified based on arguments of the existence of an extended flamelet regime.[17] A reasonable agreement between the experimental data and the LES results based on the conventional thin flame model was obtained. The present study, however, will demonstrate that the LES results are further improved in the thin reaction zone regime by adopting the broadened-flame model.

The computational domain is resolved using a resolution of $97 \times 65 \times 81$ grid points along, the axial, the radial, and the azimuthal directions, respectively. The grid was clustered in the regions of interest (such as the jet shear layer). In the earlier study[13] the accuracy of this type of coarse grid was investigated and it was determined that this resolution is reasonable for engineering level accuracy.

The numerical algorithm solves the full, unsteady, compressible Navier-Stokes equations (with the filtered G-equation and the equation for the subgrid kinetic energy) using a finite-volume code that is fourth-order accurate in space and second-order accurate in time. The localized dynamic model[25,26] was also employed. A limitation of the G-equation is that it has only two possible states: $G = 1$ denoting premixed cold fuel and $G = 0$ denoting the hot products. In the experiment, cold air is blown through the side blocks (see Fig. 2) primarily for cooling the combustor walls. However, all the combustion process is completed upstream of the air ports. To keep the net mass flow rate in the combustor unchanged, we inject hot product (with $G = 0$) through the injection port. The consequence of this injection on the combustion process occurring upstream cannot be addressed using the G-equation, however, it should not be significant.

The initial conditions were set approximately using turbulent jet profiles and, therefore, a period of time was required to wash out the effect of the initial conditions before results are collected for statistics. The inflow conditions were specified based on the normalized profiles provided by GEAE. The inflow turbulent field was generated by using a specified turbulence intensity profile (with an intensity of 7%) on randomly generated Gaussian velocity fields. At the combustor exit, characteristic outflow boundary conditions[37] were imposed. To prevent reverse flow (which will adversely affect the characteristic outflow boundary conditions) from appearing near the outflow, a buffer region was added and its area was linearly contracted by 25%. For reacting cases, the effect of the contraction on the time-averaged LES predictions was negligible as demonstrated in our earlier study.[13]

To obtain statistically stationary results for comparison with the LDV data provided by GEAE, the simulations were time-averaged for 1.5-16.2 T_{flow} as summarized in Table I. The time averaging was taken after the initial condition effects were completely washed out. It usually required an initial run of 5-10 flow-through times. Analysis showed that most of flow properties typically reaches stationary state after 5 flow-through times of time averaging. To verify this, some cases were carried out for more than three times longer than this period of time averaging. Note that for YTC time averaging was possible for only 1.5 T_{flow} because the simulation was crashed. And, as it is shown below, the results of the test models PBD10 and PBD30 were very similar to the results from PBD20. Therefore, to save computational cost, longer period of time averaging was not carried out for these test cases.

The key limiting condition for such long simulations is the availability of CPU time. The current simulations were carried out on distributed memory parallel processing computers (in particular, Cray T3E) using the Message Passing Interface (MPI). The parallelization strategy has been reported elsewhere.[13] Typically, 120 Cray T3E processors were employed primarily to reduce the turn-around time. As demonstrated earlier,[13] the present explicit LES code does scale-up very well on the Cray T3E. A typical simulation on the

Cray T3E required about 2.2 gigabytes of memory and about 1,000 single processor hours per flow-through time. Using 120 processors, it was possible to get one flow-through in about 8 (real time) hours. Thus, provided 120 processors were available a complete simulation (i.e., total 10-15 flow-through times which include 5-10 flow-through times for initial run and additional 5 flow-through times for statistics) can be completed in 10000-14000 single-processor hours which in real time is around 3-5 days. Although this appears to be quite expensive, it is worth noting that the Cray T3E is around 2-2.5 times slower than the SGI Origin 2000. Also, recent timing studies on Intel Pentium II 450 MHz PC cluster suggests that it is as fast (in terms of computational time) as the SGI Origin 2000. Thus, the continuing increase in computational speed (accompanied by drastic reduction in the cost) and the scalability of the MPI-based code used here suggest that such simulations will be feasible in 1-2 days on systems that may be more affordable in the near future.

Figure 3 compares the present LES results with available experimental data on the mean axial velocity variation along the centerline. Note that, hereafter, all velocity components (both mean and turbulence intensity) and the coordinates are nondimensionalized, respectively, using the maximum mean axial velocity at the inlet (U_0) and the inlet jet diameter (D_0). Fig. 3(a) compares three different test models which are based on Yakhot's model. Fig. 3(b) compares other three test models which are based on Pocheau's model. From these two comparisons, the effects of the broadened-flame model and the dynamic determination of the turbulent Schmidt number can be observed. Fig. 3(c) focuses on the effect of varying Pocheau's model parameter β. Conventional Yakhot's model (YTC) predicts the axial velocity variation reasonably well even though it shows some fluctuating behavior. This case, however, was numerically unstable (crashed). When the broadened-flame model is incorporated with Yakhot's model (both YBC and YBD), the simulation stabilized. These test models predict a centerline recirculation zone at $1.4 < x/D_0 < 2.8$ which was not observed in the experiment. No significant difference is found between the cases YBC and YBD.

On the other hand, conventional Pocheau's model based on the thin flame model (PTC20 and PTD20) predicts significantly higher axial velocity after the flame location at $x/D_0 = 0.81$. Again, no significant difference is found between the test models PTC20 and PTD20. Pocheau's model which is combined with the broadened-flame model (PBD20) predicts the mean axial velocity variation most accurately in comparison with the experiment. Different values of β do not significantly change this agreement as shown in Fig. 3(c). However, $\beta = 20$ is the only case which does not result in the noticeable centerline recirculation zone and, therfore, shows the best agreement with the experimental data.

Figure 4 shows the nondimensionalized mean radial velocity (W) profiles in the y-direction at $x/D_0 = 0.18$. In this comparison, most of the models behave similarly and predict the experimental data reasonably well except for PBD2. The test models based on Yakhot's model (regardless of the thin or the broadened-flame approach) result in smoother profiles than those based on Pocheau's model.

Figure 5 shows the nondimensionalized mean tangential (i.e., swirl) velocity (V) profiles in the z-direction at the same downstream location (i.e., $x/D_0 = 0.18$). All the test models result in more distinguished peaks than the experimental data. Broadened-flame versions of Yakhot's model (YBC and YBD) and Pocheau's model with $\beta = 20$ (PBD20) both show improved prediction in the entire range including the near wall region.

A similar agreement is obtained from the comparisons between the experimental data and the present LES results at further downstream locations. One of the comparisons is presented in Fig. 6 which shows the y-directional variation of the nondimensionalized mean radial velocity at $x/D_0 = 0.72$. Only the broadened-flame versions of Pocheau's model (all PBD's except for PBD2) show smooth variation of mean radial velocity profiles in the range of $-0.8 < y/D_0 < 0.8$ as is observed in the experimental data. The other models show some fluctuations in this range.

Figure 7 shows the root-mean-square (RMS) profiles of the fluctuating axial velocity components (u_{rms}) along the centerline of the combustor. The discrepancy between the experimental data and the LES results is noticeable in this comparison. The broadened-flame versions of Pocheau's model (all PBD's except for PBD2), however, still predict the experimental data better than the other test models. The discrepancy is mainly due to the inlet condition where nonphysical turbulence is prescribed. Realistic turbulence is not fed into the computational domain and, thus, for a small region turbulence has to evolve realistically. Due to this, the turbulence intensity predicted by all the LES initially drops near the inlet while the experimental data tends to remain finite there. However, since swirling jet flows are usually very unstable, realistic turbulent flows are believed to be triggered quickly near the inlet.

Since the discrepancy between the experimental data and the LES results is due to the nonphysical turbulence at the inlet, it is expected that the experiment and the LES become more comparable in the locations where inlet condition effects are not significant. Figure 8 shows one example of such locations. This plot presents the x-directional (i.e., streamwise directional) variation of u_{rms} in the corner of the

combustor, $y/D_0 = z/D_0 = 0.81$. (Note that the origin of the coordinates is the centerline point at the inlet. This y and z location,therefore, is outside the combustor inlet.) All the LES results shows an reasonable agreement with the experimental data. Main difference between the LES results appear further downstream locations where no experimental data are available therefore, it is not feasible to determine which model behaves better for this comparison.

Figure 9 shows the y-directional variation of u_{rms} at $x/D_0 = 0.18$. Again, the broadened-flame versions of Pocheau's model (all PBD's except for PBD2) show better comparison than the other test models especially near centerline region (i.e., $-0.4 < y/D_0 < 0.4$).

The other two fluctuating components show similar agreement with the experiment at this x location and at further downstream locations. Figure 10 shows one typical comparison of these components. This plot presents the y-directional RMS profiles of the fluctuating radial velocity components (w_{rms}) at $x/D_0 = 0.72$. For this comparison, all the test models based on Yakhot's model as well as the broadened-flame versions of Pocheau's model (all PBD's except for PBD2) show reasonable comparison with the experiment. Pocheau's model based on the thin flame assumption and the broadened-flame version model but using very low β (PBD2) shows the most differences when compared to the experimental data.

Arbitrarily chosen instantaneous velocity magnitude fields are shown in Figure 11. Instantaneous flame kernels are also plotted at the same instant to visualize the flame-flow interactions. These flame kernels represents the G surface where $0.45 \leq G \leq 0.55$. Both Yakhot's and Pocheau's models based on the broadened-flame assumption result in similar shape of flame kernel which is well correlated with the high-intensity velocity magnitude structures (these structures originate from the jet shear layer). On the other hand, the thin flame version models result in flame kernels which are located across the high-intensity velocity magnitude structures. As a result, the resulting velocity fields are significantly different. While most of high-intensity velocity magnitude structures are remain inside of flame kernels in the broadened-flame version models, these high-intensity velocity magnitude structures are noticeable outside the flame kernels in the thin flame versions. Also, even though the flow statistics from the dynamic model (e.g., YBD) and the constant Schmidt number model (e.g., YBC) are almost identical, instantaneous flame kernels and velocity fields are noticeably different. The dynamic model case shows much smoother profiles of both flame and velocity structures. A similar smooth profile is also observed in the broadened-flame version Pocheau's model using a low β (i.e., PBD2). As observed in the comparison of the statistics, the broadened-flame versions of Pocheau's model using reasonably high β's (i.e., PBD10, PBD20, and PBD30), show similar flame kernels and velocity structures.

7 Conclusions

A broadened-flame model for LES of turbulent premixed flames in the thin reaction zone regime has been developed. This model also has been tested by carrying out LES of high swirl and high Reynolds number turbulent jet flows in a device that is a part of a real combustor. The geometry and flow conditions of the test problem are chosen to match actual operational condition for the General Electric's lean premixed dry low NOx LM6000 combustor. It has been found that the broadened-flame model significantly improves the predictions. For example, Yakhot's model based on the conventional thin flame assumption failed (actually, the simulation has been crashed) in this particular problem. However, when the broadened-flame model was combined with Yakhot's model, the simulation stabilized and the resulting statistics agreed reasonably well with the experimental data. Overall, the best results were obtained using the broadened-flame model combined with Pocheau's model. Although the results were somewhat sensitive to the value of the model parameter β, very similar results were obtained when β was reasonably high (i.e., $10 < \beta < 30$). Note that β can be determined dynamically as a part of the simulation as described in Appendix B. In this case, LES model for premixed turbulent flows is completely closed. No parameters require *a priori* calibration or fine-tuning.

8 Acknowledgments

This work was supported in part by the Air Force Office of Scientific Research Focused Research Initiative contract F49620-95-C-0080, monitored by General Electric Aircraft Engine Company, Cincinnati, Ohio, and by the Army Research Office Multidisciplinary University Research Initiative grant DAAH04-96-1-0008. Computations were carried out under the DoD HPC Grand Challenge Project at NAVO, Stennis Space Center and ARC, Huntsville.

References

[1] Williams, F. A., "Turbulent Combustion," *The Mathematics of Combustion*, edited by J. D. Buckmaster, Society for Industrial and Applied Mathematics, 1985.

[2] Kerstein, A. R., Ashurst, W. T., and Williams, F. A., "The Field Equation for interface Propagation in an Unsteady Homogeneous Flow Field," *Physical Review A*, Vol. 37, 1988, pp. 2728–2731.

[3] Peters, N., "Laminar Flamelet Concepts in Turbulent Combustion," *Twenty-First Symposium (International) on Combustion*, 1986, pp. 1231–1250.

[4] Duclos, J. M., Veynante, D., and Poinsot, T., "A Comparison of Flamelet Models for Premixed Turbulent Combustion," *Combustion and Flame*, Vol. 95, 1993, pp. 101–117.

[5] Peters, N., "Premixed Turbulent Combustion in the Thin Reaction Zones Regime: Theory and Modelling Aspects," *Journal of Fluid Mechanics* (in press).

[6] Smith, T. M. and Menon, S., "Subgrid Combustion Modeling for Premixed Turbulent Reacting Flows," *AIAA-98-0242*, 1998.

[7] Yakhot, V., "Propagation Velocity of Premixed Turbulent Flames," *Combustion Science and Technology*, Vol. 60, 1988, pp. 191–214.

[8] Smith, T. M. and Menon, S., "One-Dimensional Simulations of Freely Propagating Turbulent Premixed Flames," *Combustion Science and Technology*, Vol. 128, 1996, pp. 99–130.

[9] Ronney, P. D. and Yakhot, V., "Flame Broadening Effects on Premixed Turbulent Flame Speed," *Combustion Science and Technology*, Vol. 86, 1992, pp. 31–43.

[10] Pocheau, A., "Scale Invariance in Turbulent Flont Propagation," *Physical Review E*, Vol. 49, 1994, pp. 1109–1122.

[11] Clavin, P. and Williams, F. A., "Theory of Premixed-Flame Propagation in Large-Scale Turbulence," *Journal of Fluid Mechanics*, Vol. 90, 1979, pp. 589–604.

[12] Chakravarthy, V. K. and Menon, S., "Large Eddy Simulation of Stationary Premixed Flames Using a Subgrid Flamelet Approach," Second AFOSR International Conference on DNS and LES, Rutgers University, June 7-9, 1999.

[13] Kim, W.-W., Menon, S., and Mongia, H. C., "Large-Eddy Simulation of a Gas Turbine Combustor Flow," *Combustion Science and Technology* (in press).

[14] Furukawa, J. and Hirano, T., "Fine Structure of Small-Scale and High-Intensity Turbulent Premixed Flames," *Twenty-Fifth Symposium (International) on Combustion*, 1994, pp. 1233–1239.

[15] Buschmann, A., Dinkelacker, F., Schäfer, T., Schäfer, M., and Wolfrum, J., "Measurement of the Instantaneous Detailed Flame Structure in Turbulent Premixed Combustion," *Twenty-Sixth Symposium (International) on Combustion*, 1996, pp. 437–445.

[16] Chen, Y.-C. and Mansour, M. S., "Investigation of Flame Broadening in Turbulent Premixed Flames in the Thin-Reaction-Zones Regime," *Twenty-Seventh Symposium (International) on Combustion*, 1998, pp. 811–818.

[17] Poinsot, T., Veynante, D., and Candel, S., "Quenching processes and premixed turbulent combustion diagrams," *Journal of Fluid Mechanics*, Vol. 228, 1991, pp. 561–606.

[18] Ronney, P. D., "Some Open Issues in Premixed Turbulent Combustion," *Modeling in Combustion Science Proceedings of the US-Japan Seminar, Kapaa, Kauai, Hawaii, 24-29 July*, edited by J. Buckmaster and T. Takeno, Springer-Verlag, 1994, pp. 3–22.

[19] Smagorinsky, J., "General Circulation Experiments with the Primitive Equations," *Monthly Weather Review*, Vol. 91, No. 3, 1963, pp. 99–164.

[20] Schumann, U., "Subgrid Scale Model for Finite Difference Simulations of turbulent Flows in Plane Channels and Annuli," *Journal of Computational Physics*, Vol. 18, 1975, pp. 376–404.

[21] Fureby, C., "Towards Large Eddy Simulations of Flows in Complex Geometries," *AIAA-98-2806*, 1998.

[22] Germano, M., Piomelli, U., Moin, P., and Cabot, W. H., "A Dynamic Subgrid-Scale Eddy viscosity Model," *Physics of Fluids A*, Vol. 3, No. 11, 1991, pp. 1760–1765.

[23] Damköhler, G., "The Effect of Turbulence on the Flame Velocity in Gas Mixtures," *Zeitschrift Elektrochem., English translation, NACA Tech. Memo. No. 1112 1947*, Vol. 46, 1940, pp. 601.

[24] Yakhot, V. and Orszag, S. A., "Renormalization Group Analysis of Turbulence. I. Basic Theory," *Journal of Scientific Computing*, Vol. 1, No. 1, 1986, pp. 3–51.

[25] Kim, W.-W. and Menon, S., "A New Dynamic One-Equation Subgrid-Scale Model for Large-Eddy Simulations," *AIAA-95-0356*, 1995.

[26] Kim, W.-W. and Menon, S., "An Unsteady Incompressible Navier-Stokes Solver for Large-Eddy Simulation of Turbulent Flows," *International Journal for Numerical Methods in Fluids* (in press).

[27] Pope, S. B. and Anand, M. S., "Flamelet and Distributed Combustion in Premixed Turbulent Flames," *Twentieth Symposium (International) on Combustion*, 1984, pp. 403–410.

[28] Abdel-Gayed, R. G., Al-Khishali, K. J., and Bradley, D., "Turbulent Burning Velocities and Flame Straining in Explosions," *Proceedings of the Royal Society London A*, Vol. 39, 1984, pp. 393–414.

[29] Hinze, J. O., *Turbulence*, McGraw-Hill Book Company, 2nd ed., 1975.

[30] Seshadri, K. and Peters, N., "The Inner Structure of Methane-Air Flames," *Combustion and Flame*, Vol. 81, 1990, pp. 96–118.

[31] Abdel-Gayed, R. G. and Bradley, D., "Criteria for Turbulent Propagation Limits of Premixed Flames," *Combustion and Flame*, Vol. 62, 1985, pp. 61–68.

[32] Abdel-Gayed, R. G. and Bradley, D., "Combustion Regimes and the Straining of Turbulent Premixed Flames," *Combustion and Flame*, Vol. 76, 1989, pp. 213–218.

[33] Abdel-Gayed, R. G., Bradley, D., and Lawes, M., "Turbulent Burning Velocities: a General Correlation in Terms of Straining Rates," *Proceedings of the Royal Society London A*, Vol. 414, 1987, pp. 389–413.

[34] Cheng, R. K., "Velocity and Scalar Characteristics of Premixed Turbulent Flames stabilized by Weak Swirl," *Combustion and Flame*, Vol. 101, 1995, pp. 1–14.

[35] Joshi, N. D., Mongia, H. C., Leonard, G., Stegmaier, J. W., and Vickers, E. C., "Dry Low Emissions Combustor Development," *ASME-98-GT-310*, 1998.

[36] Kim, W.-W., Menon, S., and Mongia, H. C., "Large Eddy Simulations of Reacting Flow in a Dump Combustor," *AIAA-98-2432*, 1998.

[37] Poinsot, T., Echekki, T., and Mungal, M. G., "A Study of the Laminar Flame Tip and Implications for Premixed Turbulent Combustion," *Combustion Science and Technology*, Vol. 81, 1992, pp. 45–73.

[38] Erlebacher, G., Hussaini, M. Y., Speziale, C. G., and Zang, T. A., "Toward the Large-Eddy Simulation of Compressible Turbulent Flows," *Journal of Fluid Mechanics*, Vol. 238, 1992, pp. 155–185.

[39] Menon, S., Yeung, P.-K., and Kim, W.-W., "Effect of Subgrid Models on the Computed Interscale Energy Transfer in Isotropic Turbulence," *Computers and Fluids*, Vol. 25, No. 2, 1996, pp. 165–180.

[40] Kim, W.-W. and Menon, S., "Numerical Modeling of Fuel/Air Mixing in a Dry Low-Emission Premixer," Second AFOSR International Conference on DNS and LES, Rutgers University, June 7-9, 1999.

A Subgrid Closure for Momentum Equations

Spatial filtering reduces the high wave number Fourier components of the flow variables and separates the resolved scale components from the unresolved scales. Following earlier study,[38] the flow variables are decomposed into the resolved (supergrid scale) and unresolved (subgrid scale) components by a spatial filtering operation. The Favre filtered variable is defined as,

$$\widetilde{f} = \frac{\overline{\rho f}}{\overline{\rho}} \tag{32}$$

where the over bar represents a spatial filtering which is defined as,

$$\overline{f(x_i,t)} = \int f(x_i',t) G_f(x_i, x_i') dx_i'. \tag{33}$$

Here, t is the time, x_i $(i = 1,2,3)$ is the coordinate, and G_f is the filter kernel and the integral is extended over the entire domain. Applying the filtering operation (in the present study, a low-pass filter of the computational mesh is used, hence, the characteristic size of this filter is the grid width $\overline{\Delta}$) to the Navier-Stokes equations, the following unclosed subgrid term representing the subgrid stress tensor appears in the filtered momentum equation:

$$\tau_{ij}^{sgs} = \overline{\rho}[\widetilde{u_i u_j} - \widetilde{u}_i \widetilde{u}_j]. \tag{34}$$

This term can be modeled using the subgrid kinetic energy which is obtained by solving the following transport equation:[39]

$$\frac{\partial \overline{\rho} k^{sgs}}{\partial t} + \frac{\partial}{\partial x_i}(\overline{\rho}\widetilde{u}_i k^{sgs}) = P^{sgs} - \varepsilon^{sgs} + \frac{\partial}{\partial x_i}\left(\frac{\overline{\rho}\nu_t}{Pr_t}\frac{\partial k^{sgs}}{\partial x_i}\right) \tag{35}$$

where Pr_t is the turbulent Prandtl number. The terms on the right side of Eq. (35) represent, respectively, the production, the dissipation, and the transport of the subgrid kinetic energy. The production term is modeled as $P^{sgs} = -\tau_{ij}^{sgs}(\partial\widetilde{u}_i/\partial x_j)$ where the subgrid shear stresses τ_{ij}^{sgs} are evaluated as,

$$\tau_{ij}^{sgs} = -2\overline{\rho}\nu_t(\widetilde{S}_{ij} - \frac{1}{3}\widetilde{S}_{kk}\delta_{ij}) + \frac{2}{3}\overline{\rho}k^{sgs}\delta_{ij}. \tag{36}$$

Here, ν_t is the subgrid eddy viscosity given by $\nu_t = C_\nu(k^{sgs})^{1/2}\overline{\Delta}$ and $\widetilde{S}_{ij} = \frac{1}{2}(\partial\widetilde{u}_i/\partial x_j + \partial\widetilde{u}_j/\partial x_i)$ is the resolved-scale rate-of-strain tensor. The dissipation term is modeled as $\varepsilon^{sgs} = C_\varepsilon\overline{\rho}(k^{sgs})^{3/2}/\overline{\Delta}$, where, $\overline{\Delta}$ is a characteristic grid size. The two coefficients appearing in the above equations, C_ν and C_ε, can determined dynamically as a part of the solutions of the LES. The localized dynamic k-equation model (LDKM) proposed by Kim and Menon[25] is one of a few dynamic models whose capability has been proven both for reacting and nonreacting turbulent flow simulations. A detailed description of the LDKM and its

application to various turbulent flows can be found elsewhere[25,26,40] and, therefore, is avoided here for brevity.

B Dynamic Closure for G-Equation

The dynamic procedure used in the LDKM can be extended to close the G-equation. As in other dynamic models,[22] the LDKM is also based on the assumption of scale similarity in the inertial subrange. Provided that enough of the inertial subrange is resolved, unclosed terms at the cutoff (i.e., the grid size) can be related to similarly defined terms at say twice the cutoff (i.e., the test filter width). This then defines a scale level where explicit filtering is required. The test-scale field is constructed from the grid-scale field by applying a test filter which is characterized by $\widehat{\Delta}$ (typically, $\widehat{\Delta} = 2\overline{\Delta}$). Hereafter, the application of the test filter on any variable ϕ is denoted by $\widehat{\phi}$ and the test-scale Favre-filtered variable is denoted by $< \phi >= \widehat{\overline{\rho}\phi}/\widehat{\overline{\rho}}$.

As shown in (3), two unclosed terms were produced by filtering the G-equation. The model for G_i^{sgs} in (4) includes a turbulent Schmidt number Sc^G which can be determined using a dynamic procedure. By assuming the scale similarity, a similar term can be defined at the test-filter level and this term can be closed using the quantities defined at the same level:

$$G_i^{test} = \widehat{\overline{\rho}}\left[\left\langle \widetilde{u}_i\widetilde{G}\right\rangle - \left\langle \widetilde{u}_i\right\rangle\left\langle \widetilde{G}\right\rangle\right] \approx -C_s\widehat{\overline{\rho}}\nu_t^{test}\frac{\partial\left\langle \widetilde{G}\right\rangle}{\partial x_i} \tag{37}$$

where $C_s = 1/Sc^G$, $\nu_t^{test} = C_\nu\left(k^{test}\right)^{1/2}\widehat{\Delta}$, and $k^{test} = \frac{1}{2}\left(\left\langle \widetilde{u}_k\widetilde{u}_k\right\rangle - \left\langle \widetilde{u}_k\right\rangle\left\langle \widetilde{u}_k\right\rangle\right)$ is the resolved kinetic energy at the test-filter level. From this equation, C_s can be directly evaluated:

$$C_s = \frac{-G_i^{test}}{\nu_t^{test}\left|\nabla\left\langle \widetilde{G}\right\rangle\right|^2}\frac{\partial\left\langle \widetilde{G}\right\rangle}{\partial x_i}. \tag{38}$$

In the model for S^{sgs} in(5), the only unknown quantity is S_T and this quantity can be determined by employing the turbulent flame speed models. Most of turbulent flame speed models except for Yakhot's model[7] include an adjustable parameter. Presently, we use the turbulent flame speed model introduced by Pocheau.[10] Similarly as S^{sgs}, S^{test} can be defined at the test-filter level and it also can be modeled using the quantities defined at the test scale.

$$S^{test} = \widehat{\overline{\rho}\widetilde{S_L}\left|\nabla\widetilde{G}\right|} \approx \rho_0 S_T^{test}\left|\nabla\left\langle \widetilde{G}\right\rangle\right|. \tag{39}$$

Here, $\widetilde{S_L}$ is the grid-filtered laminar flame speed and is generally not a constant. $\widetilde{S_L}$ varies due to the effect of flame stretch and its expression is obtained by introducing the Markstein length $\mathcal{L}_M$:

$$\widetilde{S_L} = S_L^0 - S_L^0\mathcal{L}_M\frac{\nabla^2\widetilde{G}}{\left|\nabla\widetilde{G}\right|} + S_L^0\mathcal{L}_M\frac{\partial\ln\left|\nabla\widetilde{G}\right|}{\partial x_j}\frac{\partial\widetilde{G}}{\partial x_j}\frac{1}{\left|\nabla\widetilde{G}\right|} + \mathcal{L}_M\frac{1}{\left|\nabla\widetilde{G}\right|^2}\frac{\widetilde{u_k}}{\partial x_j}\frac{\widetilde{G}}{\partial x_j}\frac{\widetilde{G}}{\partial x_k}. \tag{40}$$

The turbulent flame speed model also can be applied to the test-filter level (presently, Pocheau's model is adopted):

$$\left(\frac{S_T^{test}}{S_L^0}\right)^\gamma = 1 + \beta\left(\frac{u'^{test}}{S_L^0}\right)^\gamma \tag{41}$$

where $u'^{test} = \left[2\left(k^{test} + k^{sgs}\right)/3\right]^{1/2}$. Finally, by combining these relations, β can be evaluated as a part of LES solutions (i.e., dynamically):

$$\beta = \left(\frac{S_L^0}{u'^{test}}\right)^\gamma\left[\left(\frac{\widehat{\overline{\rho}\widetilde{S_L}\left|\nabla\widetilde{G}\right|}}{\rho_0 S_L^0\left|\nabla\left\langle \widetilde{G}\right\rangle\right|}\right)^\gamma - 1\right]. \tag{42}$$

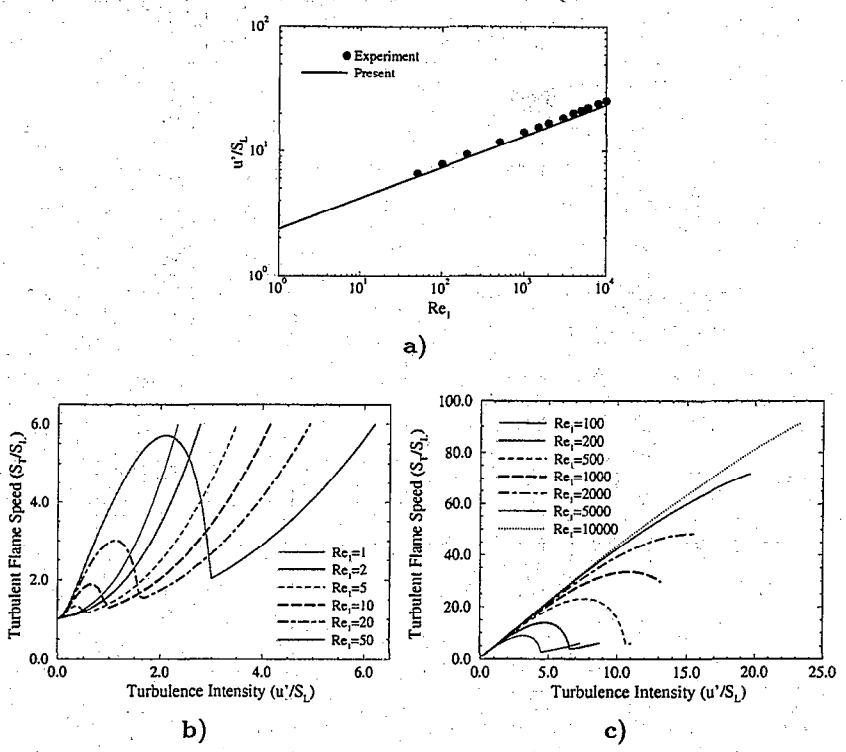

Fig. 1 (a) Comparison of the predicted flamelet limit with the quenching limit observed in experiments; (b) and (c) turbulent flame speed (S_T/S_L) plots.

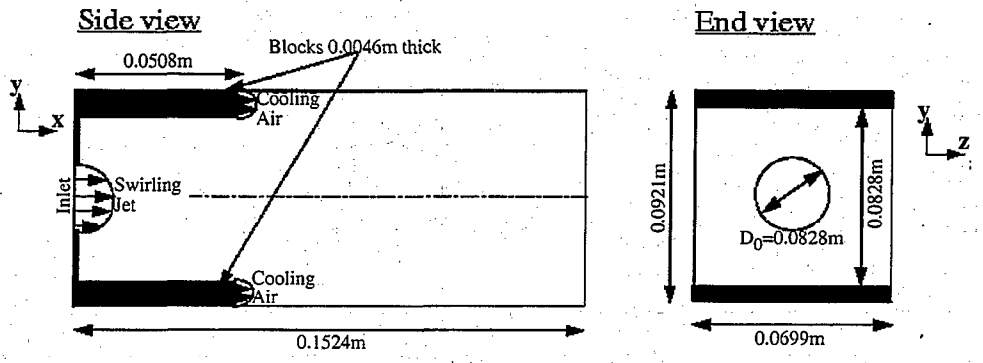

Fig. 2 Schematic of GE's lean premixed dry low NOx gas turbine combustor.

Table I. Summary of test models.

Test Models	Yakhot(Y) or Pocheau(P)'s	Broadened(B) or Thin(T) flame	Dynamic(D) or Constant(C) Sc^G	β	Time-Average Period (T_{flow})
YTC	Y	T	C	NA	1.5
YBC	Y	B	C	NA	6.6
YBD	Y	B	D	NA	16.2
PTC20	P	T	C	20	14.0
PTD20	P	T	D	20	7.9
PBD20	P	B	D	20	6.0
PBD2	P	B	D	2	3.6
PBD10	P	B	D	10	2.0
PBD30	P	B	D	30	3.3

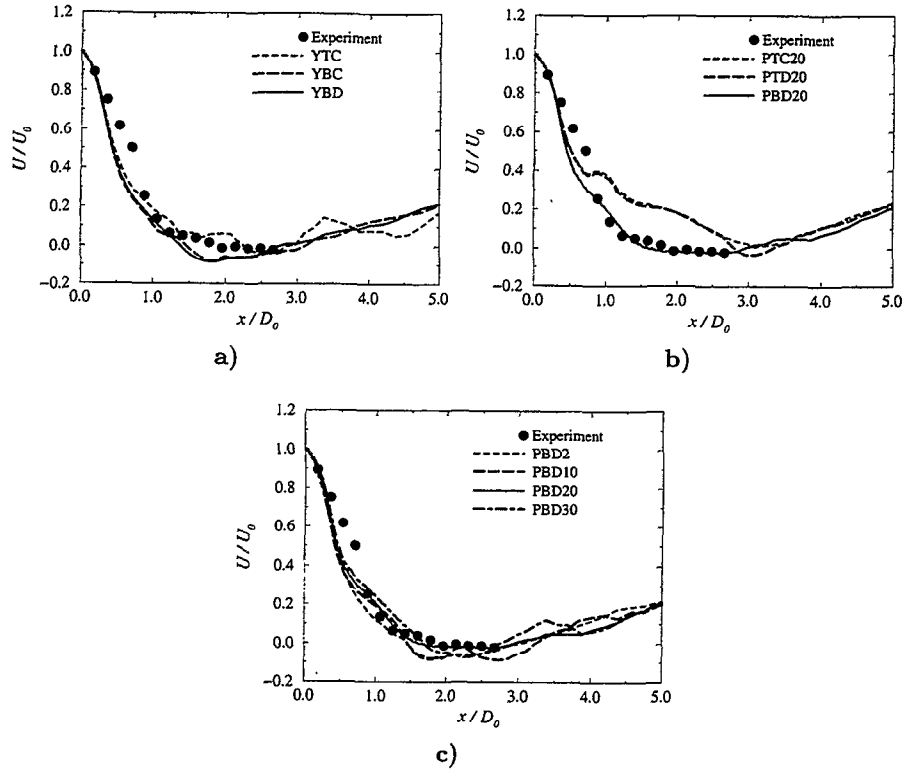

Fig. 3 Comparison of the predicted mean axial velocity variation and experimental data along the combustor centerline.

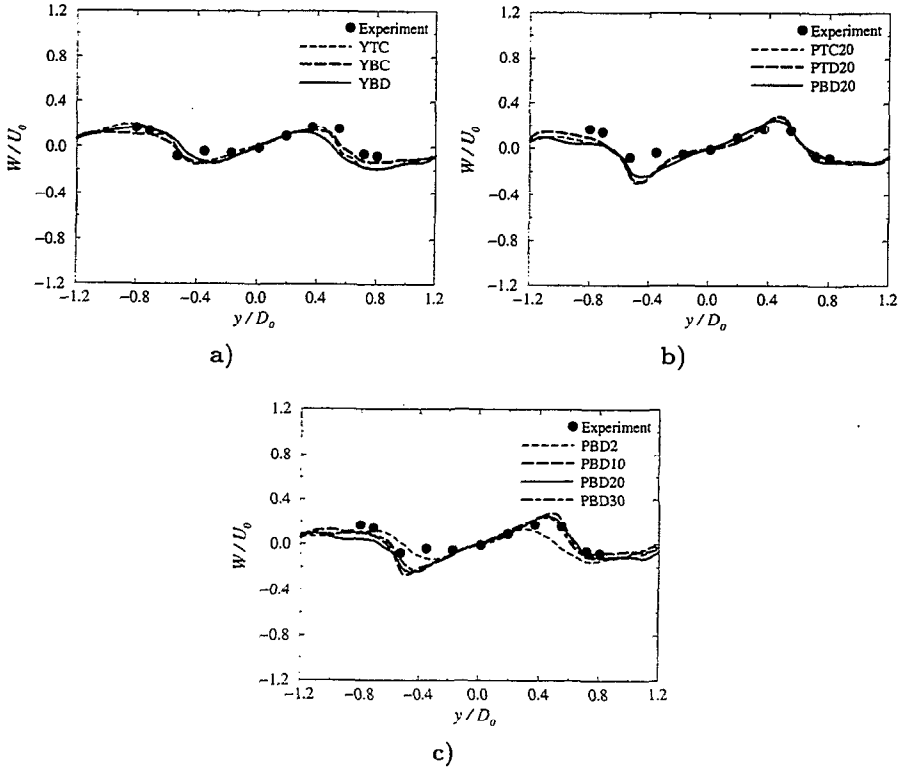

Fig. 4 Comparison of the predicted mean radial velocity variation and experimental data along the y-axis at $x/D_0 = 0.18$.

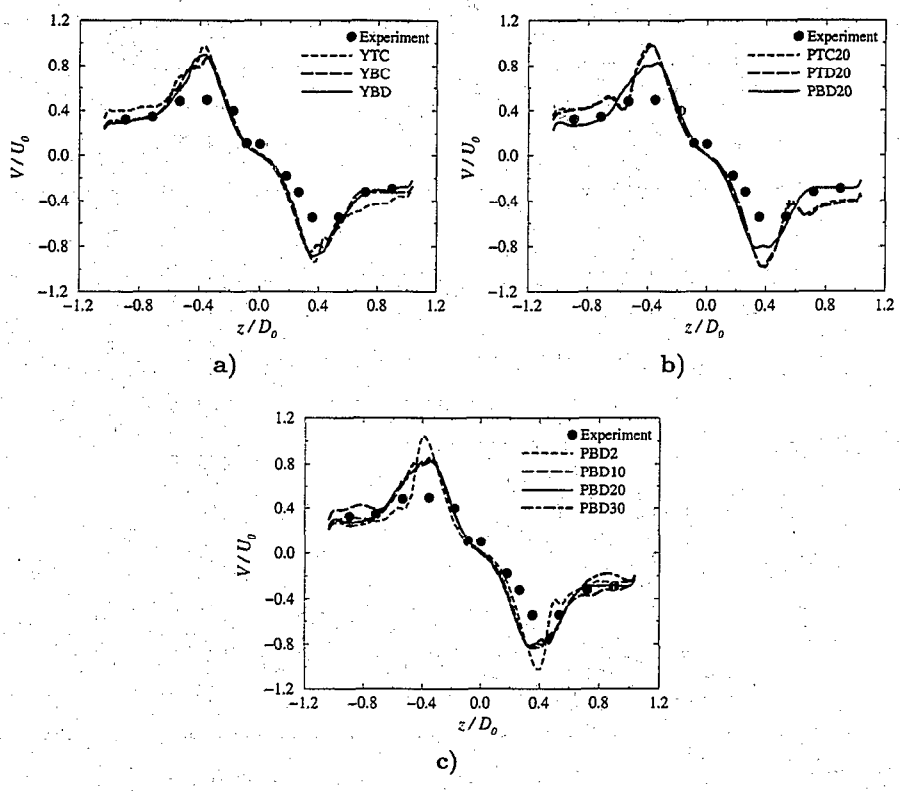

Fig. 5 Comparison of the predicted mean tangential (swirl) velocity variation and experimental data along the z-axis at $x/D_0 = 0.18$.

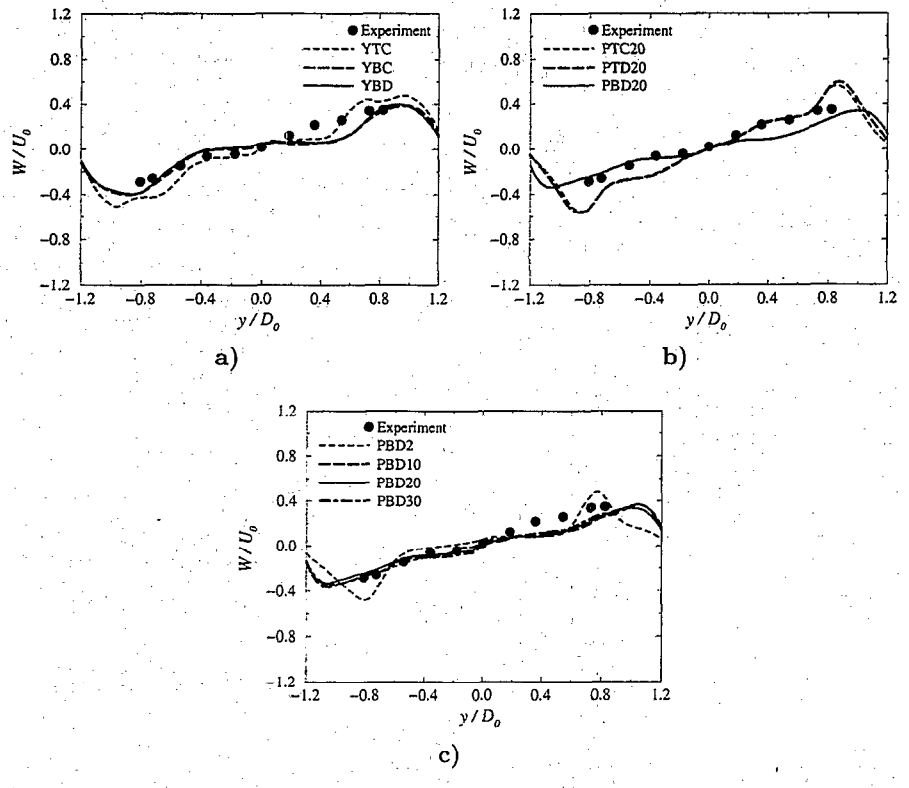

Fig. 6 Comparison of the predicted mean radial velocity variation and experimental data along the y-axis at $x/D_0 = 0.72$.

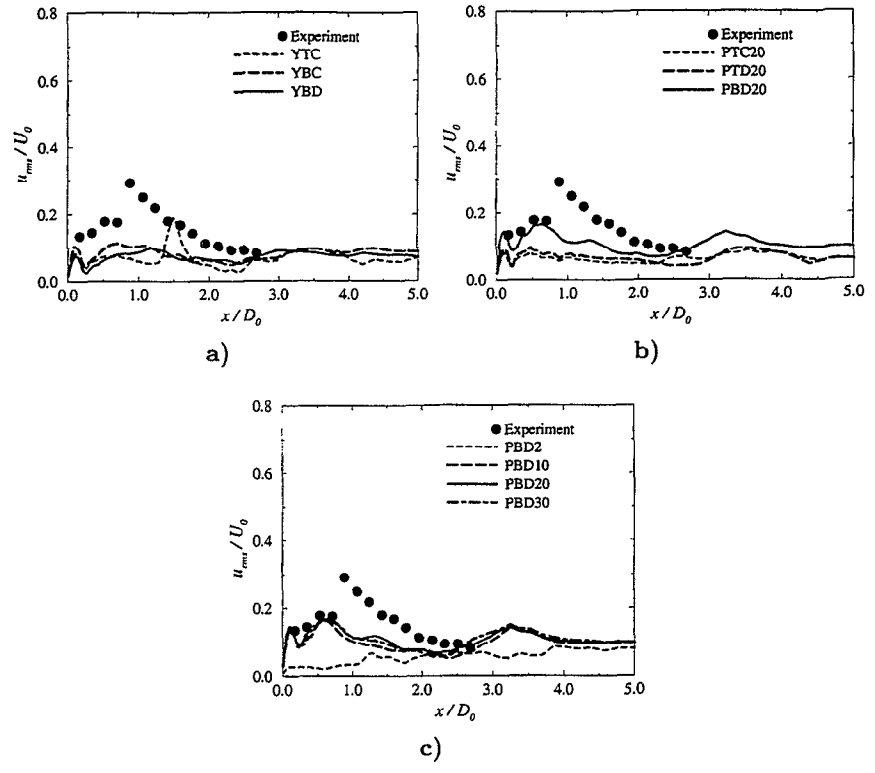

Fig. 7 Comparison of the predicted axial velocity fluctuation intensity and experimental data along the combustor centerline.

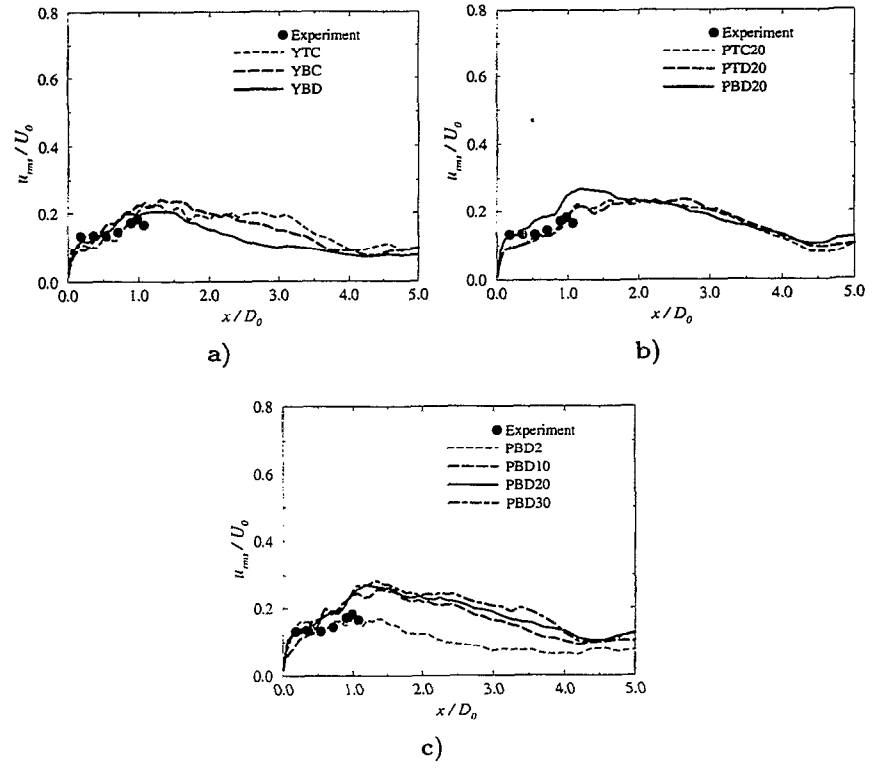

Fig. 8 Comparison of the predicted axial velocity fluctuation intensity and experimental data along the x-axis at $y/D_0 = z/D_0 = 0.81$.

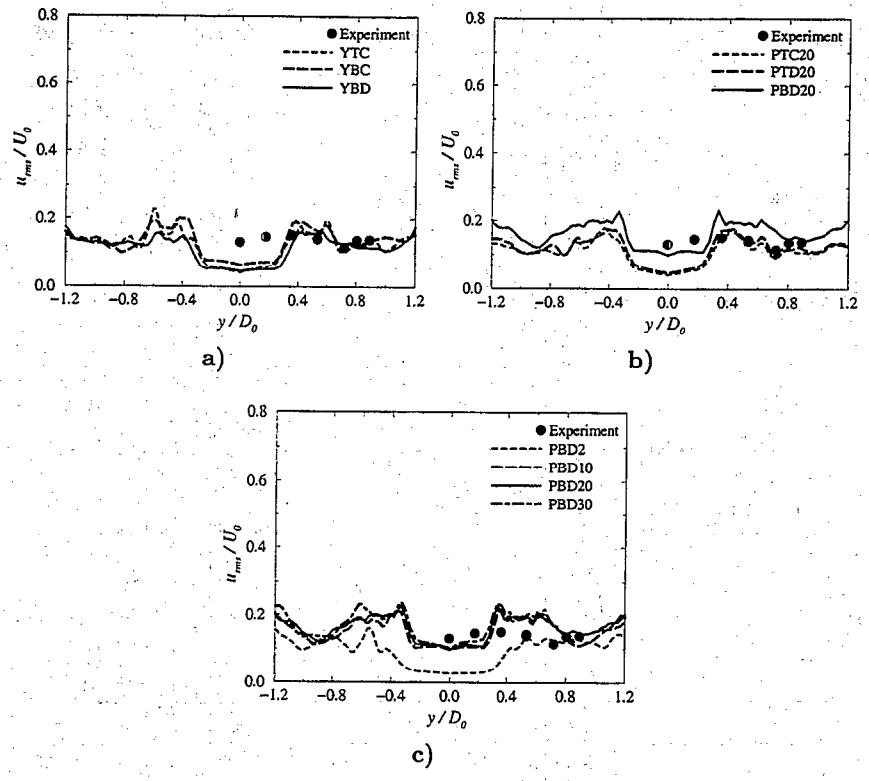

Fig. 9 Comparison of the predicted axial velocity fluctuation intensity and experimental data along the y-axis at $x/D_0 = 0.18$.

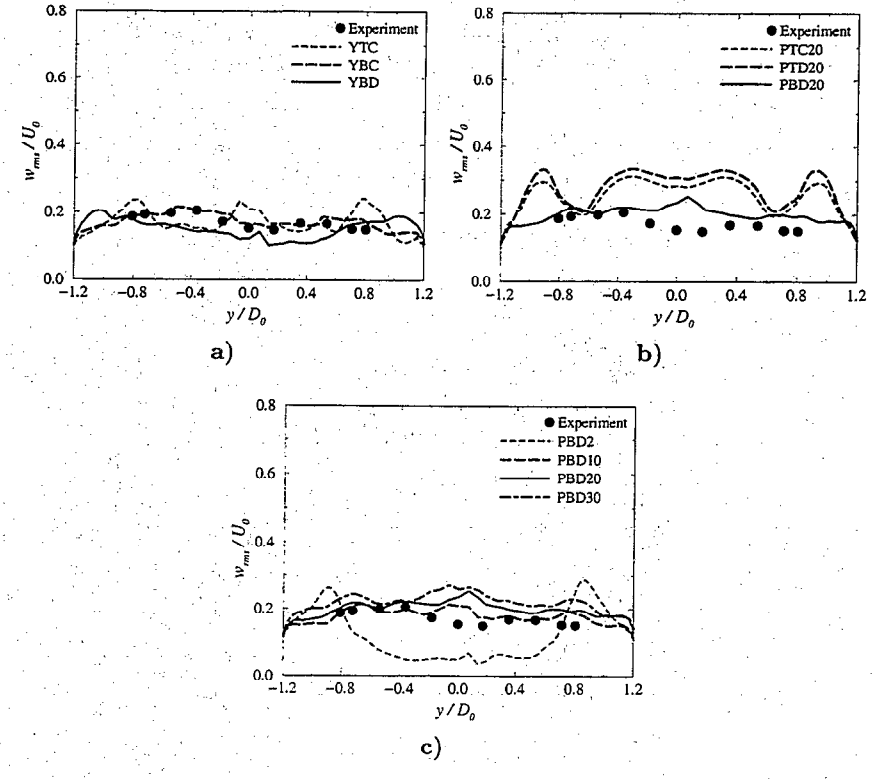

Fig. 10 Comparison of the predicted radial velocity fluctuation intensity and experimental data along the y-axis at $x/D_0 = 0.72$.

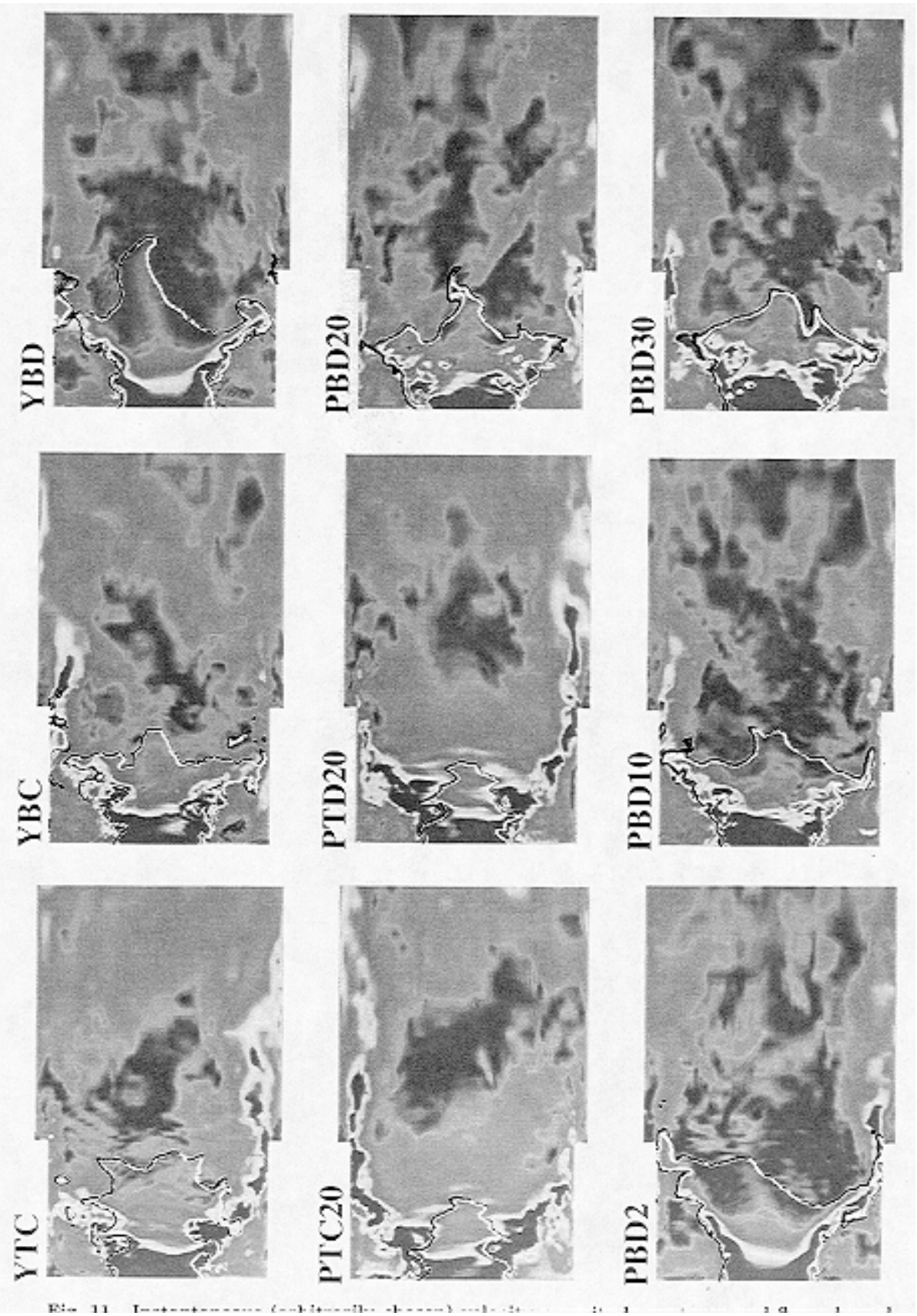

Fig. 11 Instantaneous (arbitrarily chosen) velocity magnitude contours and flame kernel